

1 **Numerical validation of the incremental launching method of a steel bridge through a small**
2 **scale experimental study**

3 R. Chacón*, N. Uribe*, S. Oller**

4 *Construction Engineering Department

5 **International Centre for Numerical Methods in Engineering (CIMNE)

6 Universitat Politècnica de Catalunya. Barcelona Tech

7 Submitted for copyediting and typesetting in

8 Experimental Techniques

9
10 **Abstract**

11 *This paper presents an experimental and a numerical study of an incremental launching process*
12 *of a steel bridge. The former is deployed in a scale-reduced laboratory whereas the latter, is*
13 *performed using the finite element method. The numerical simulation is based upon realistic*
14 *transient boundary conditions and accurately reproduces the elastic response of the steel bridge*
15 *during launching. This numerical approach is validated experimentally with the scale-reduced*
16 *test performed at the laboratory. The properly validated numerical model is subsequently*
17 *systematically employed as a simulation tool of the process. The proposed simulation protocol*
18 *might be useful for design and monitoring purposes of steel bridges to be launched. Results*
19 *concerning strains, stresses and displacements might be inferred from the model and thus*
20 *compared to field measurements obtained in situ. The conditions presented at the end of the*
21 *paper are potentially useful for researchers and practice engineers alike.*

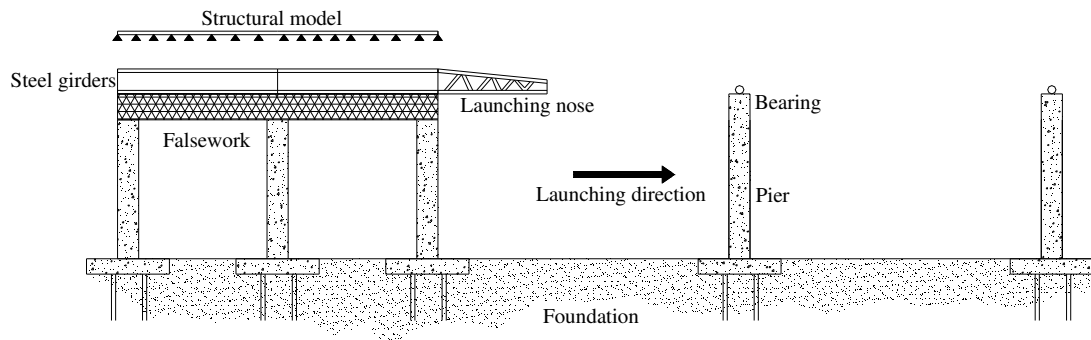
22
23
24 **Keywords:** Incremental launching method. Steel bridges. Bridge monitoring

25 **1. Introduction**

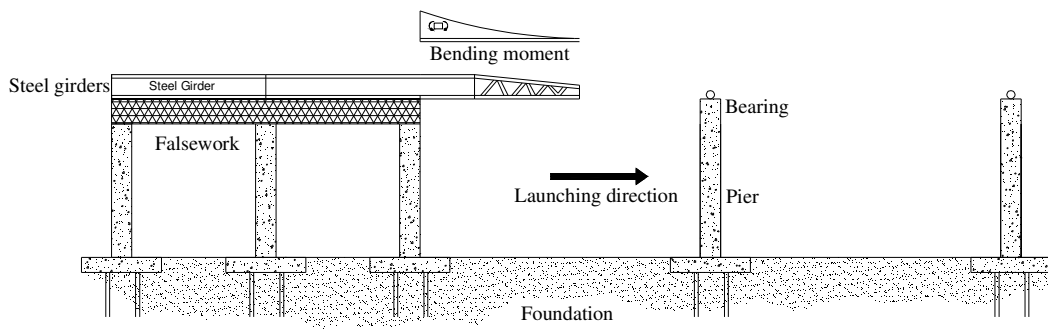
26 The incremental launching method (ILM) has gained increasing popularity in last decades as a
27 construction method of short- to large- multi-spanned steel and/or concrete bridges [1]. ILM
28 consists of assembling the superstructure on one side of the obstacle to be crossed and then
29 pushed longitudinally (or “launched”) into its final position. Generally, steel bridges are
30 completely assembled prior to launching operations. In concrete bridges, however, the launching
31 is typically performed in a series of increments so that additional sections can be added to the
32 rear of the superstructure unit prior to subsequent launches. The ILM may offer advantages over
33 conventional construction techniques when the construction takes place in environmentally
34 protected areas, or areas at which minimal disturbances to surroundings are needed, thus
35 providing a more concentrated work area for the superstructure assembly. Safety concerns might
36 also be reduced if ILM is employed [1-3]. During the launching operation, the bridge
37 superstructure is supported by a series of rollers or sliding bearings. The thrust required to launch
38 the bridge forward can be provided by a variety of jacking systems, including hydraulic pistons
39 or hollow-core strand jacks [1]. Fig. 1 shows a lateral schematic view of an incrementally
40 launched steel girder. It is worth pointing out the continuous change of the static conditions. In
41 Fig. 1, the varying bending moment diagrams are qualitatively included for illustration.

42

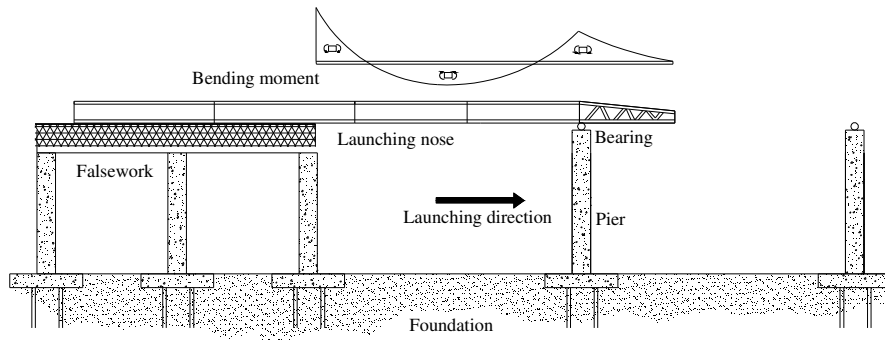
43



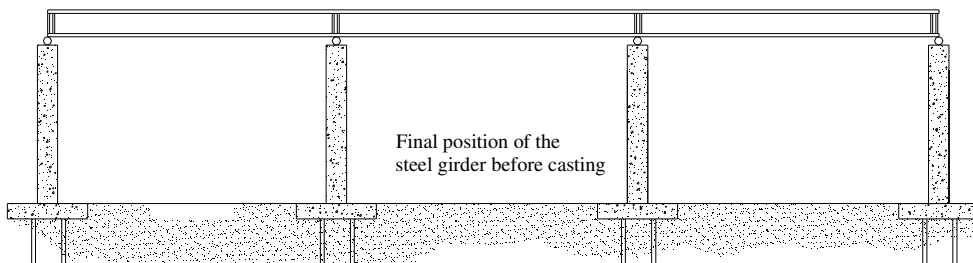
44



45



46



47

48

Figure 1. Incremental launching method of a steel bridge.

49 ILM has reportedly been used for the first time in Venezuela during the sixties for a bridge over
50 the Caroni River [3]. Ever since that, hundreds of steel and/or concrete bridges have been built
51 worldwide using the ILM. A close inspection of the vast database given in [1] gives a worth
52 mentioning twofold observation: Europe has a vaster tradition of systematic usage of ILM than
53 the U.S.A and the vast majority of launched bridges are made of post-tensioned concrete.

54

55 Admittedly, according to [1], there has historically been a knowledge gap between designers,
56 contractors and bridge owners when it comes to the systematic usage of ILM. ILM requires a
57 considerable amount of analysis and design expertise and specialized construction equipment. A
58 detailed structural analysis of all construction phases is compulsory. It is necessary to take into
59 account the continuous change of the structural scheme due to the transient conditions of the
60 supports. Internal as well as external forces acting on the rollers might considerably change
61 throughout the process. The stress state at the final phase of the bridge girders might differ
62 considerably (in magnitude and sign) from the stress states that have been carried out during
63 launching. Furthermore, it is a matter of fact that the launching of bridges made of concrete
64 requires a different set of solutions than those required for purely metallic bridges. For the
65 former, the design of the post-tensioning system must consider not only dead load stresses, but
66 also the considerable stress reversals that occur during launching. For the latter, there are a
67 number of issues related to large concentrated forces applied to the girder (namely, patch
68 loading) as well as to the torsional stiffness of an open section, such as an I-girder, that must be
69 carefully addressed by the designer in order to avoid an undesired instability-related collapse.

70

71 This paper presents numerical and scale-reduced experimental reproductions of a steel bridge
72 whose construction process is the ILM. The numerical reproduction is performed using a FE-
73 based commercial Software that is properly validated with a scale-reduced model deployed at the
74 Laboratory of the Chair of Strength of Materials-Technical University of Catalonia (UPC). The
75 numerical model is based upon a contact formulation and allows to reproduce the continuous
76 change of the boundary conditions of the launched girders. The results provided by the numerical
77 model include stresses, strains, displacements and support reactions that might be compared *in*
78 *situ* to field measurements during the whole process. These comparisons might be of the utmost
79 importance for control and monitoring engineers. Consequently, the results presented at the end
80 of the paper are aimed at showing relevant information for designers, contractors and bridge
81 owners alike.

82

83 **2. State of the art**

84 The ILM has been depicted quite thoroughly during the last decades in several books and papers
85 available in the literature that address this topic with a broad perspective [1-6]. More specific
86 papers concerning particular topics of the method have continuously been published. Rosignoli
87 has focused his research to the design of the bridges, the launching noses and the rolling devices
88 [7-11] whereas Granath has pointed out the structural response of particular elements of the steel
89 bridges that are exposed to concentrated loads of considerable magnitude [12-14]. On the other
90 hand, several publications related to bridges constructed using the ILM are available [1] [15-17].

91

92 Publications related to the numerical simulation of incrementally launched steel bridges are,
93 however, rather scarce. Marzouk et al [18] performed several applications of computer

94 simulations of incrementally launched bridges. Their main purpose was to improve the design of
95 the bridge to be launched by developing optimization algorithms. Ronggiao and Shao [19]
96 developed a new beam finite element suitable to reproduce the continuous changes in the support
97 conditions when a superstructure is constructed using the ILM.
98 Moreover, it has been of the utmost importance to monitor steel bridges while being launched.
99 During the launching phase, the process is usually monitored via reaction at supports/rollers or
100 via displacement using topography equipment [2]. These controls are discretely measured in
101 regions that are anticipated to be somewhat critical. Recently, Chacón et al. [20] performed a
102 research work aimed at monitoring the strain levels of the steel girders with wireless sensors. The
103 results have been useful at research levels showing that wireless technology might be
104 considerably useful during such construction process. Other researchers have already
105 implemented monitoring deployments over incrementally launched steel bridges with various
106 levels of accuracy and/or amount of collected data [21-23]. Publications related to computer-aid
107 design and visualization of launched bridges are also available [24].

108

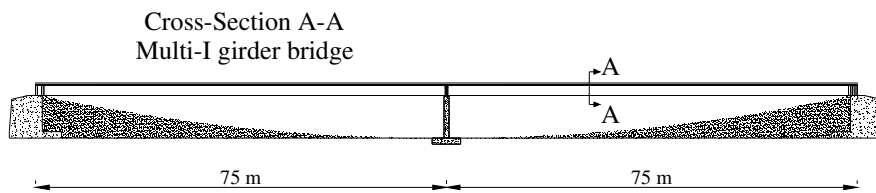
109 **3. Scale-reduced experimental simulation of the ILM**

110 3.1 General

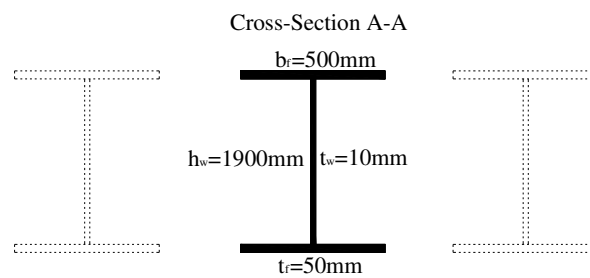
111 An experimental reproduction of an incremental launching procedure of a steel bridge was
112 deployed at the Laboratory of the Chair of Strength of Materials-Technical University of
113 Catalonia (UPC). The objective was to reproduce a launching procedure of a medium- multi-
114 spanned bridge assembled with steel I-girders. This prototype is a standard design routinely
115 employed in road bridges [25]. The chosen geometry for the reproduction is a laterally-
116 restrained, steel multi-I-girder whose final configuration is a continuous and symmetric two-

117 spanned multi I-girder beam with a total length of 150 meters and a single central pier (Fig.2).
118 The generic cross-section dimensions of the analyzed girder are also included. For the sake of
119 simplicity, only one girder (bolded in Fig. 2) is considered in the analysis. The other girders are
120 displayed in dashed lines only for illustration purposes.

121



122



123

124

Figure 2. Prototype longitudinal and transversal view.

125

126 The depicted prototype was scale-reduced for a proper adaptation to the laboratory facilities. The
127 reduced model was inferred from a thorough comparison between the prototype geometry, the
128 laboratory facilities and by applying the PI-Buckingham theorem [26-27]. The theorem roughly
129 states that a physically meaningful equation (in this case, structurally meaningful) involving a
130 certain number n of parameters is equivalent to an equation involving a set of $p = n -$
131 k dimensionless parameters constructed from the original variable (being k the number of
132 independent fundamental physical quantities).

133 Table 1 shows the considered "n" structural parameters (including numerical values) whereas
 134 Table 2 shows the "p" chosen dimensionless groups. Thus, the prototype was structurally scale-
 135 reduced to the experimental model

Symbol	Description	SI units	Prototype	Scale reduced model
E	Elasticity modulus	N/mm ²	210000	210000
ν	Poisson's ratio	-	0,3	0,3
L	Span length	m	75	1
Q	Self-weight	kN/m	5,42	$1,88 \cdot 10^{-2}$
M	Bending moment	kN-m	15,23	$9,42 \cdot 10^{-3}$
σ	Stress	N/mm ²	286	58,9
ϵ	Strain	-	$1,43 \cdot 10^{-3}$	$2,94 \cdot 10^{-4}$
δ	Vertical displacement	mm	2010	37
φ	Rotations at supports	rad	$3,58 \cdot 10^{-2}$	$4,91 \cdot 10^{-2}$
W	Section modulus	mm ³	53257,5	160
F	Forces (Reactions)	kN	406,24	$1,88 \cdot 10^{-2}$

136 **Table 1. Structural parameters.**

137

138

139

140

141

Dimensionless Group	Similarity	Structural parameters	Dimensionless ratios	Scale factor
1	$\pi_1 = \pi'_1$	$\frac{F}{E \cdot l^2} = \frac{F'}{E' \cdot l'^2}$	$\lambda_f = \lambda_l^2$	$\left(\frac{1}{75}\right)^2$
2	$\pi_2 = \pi'_2$	$v = v'$	$\lambda_v = 1$	1
3	$\pi_3 = \pi'_3$	$\frac{q}{E \cdot L} = \frac{q'}{E' \cdot L'}$	$\lambda_l = \lambda_q$	$\left(\frac{1}{75}\right)$
4	$\pi_3 = \pi'_3$	$\frac{M}{p \cdot l} = \frac{M'}{p' \cdot l'}$	$\lambda_M = \lambda_l$	$\left(\frac{1}{75}\right)$
5	$\pi_5 = \pi'_5$	$\sigma = \sigma'$	$\lambda_\sigma = 1$	1
6	$\pi_6 = \pi'_6$	$\varepsilon = \varepsilon'$	$\lambda_\varepsilon = 1$	1
7	$\pi_7 = \pi'_7$	$\frac{\delta}{l} = \frac{\delta'}{l'}$	$\lambda_\delta = \lambda_l$	$\frac{1}{75}$
8	$\pi_8 = \pi'_8$	$\phi = \phi'$	$\lambda_\phi = 1$	1
9	$\pi_9 = \pi'_9$	$\frac{l^3}{w} = \frac{l'^3}{w'}$	$\lambda_w = \lambda_l^3$	$\left(\frac{1}{75}\right)^3$

Table 2. Dimensionless groups and similarity ratios.

143

144

145 A close inspection of Tables 1 and 2 leads to pinpoint a threefold observation:

- 146 • Dimensionless groups 7 and 9 define the scale-reduced model geometry, that is to say,
147 the ratio between vertical displacement and the span length.
- 148
- 149 • The self-weight is not considered in the structural variables as a mass force. The
150 prototype and the scale-reduced model are made of the same material (steel). Therefore,
151 both have identical values of density, Young's modulus and Poisson's ratio.

152

- 153 • Strains, stresses, and Poisson's ratio (groups 2,5 and 6) remained unaltered in the
154 reduced model. These magnitudes do not play any role when calculating the scaled
155 model geometry. However, from a simplified static analysis of the phenomenon, it was
156 inferred and verified that the stresses obtained at any point on the steel plate should not
157 exceed the yield point threshold.

158

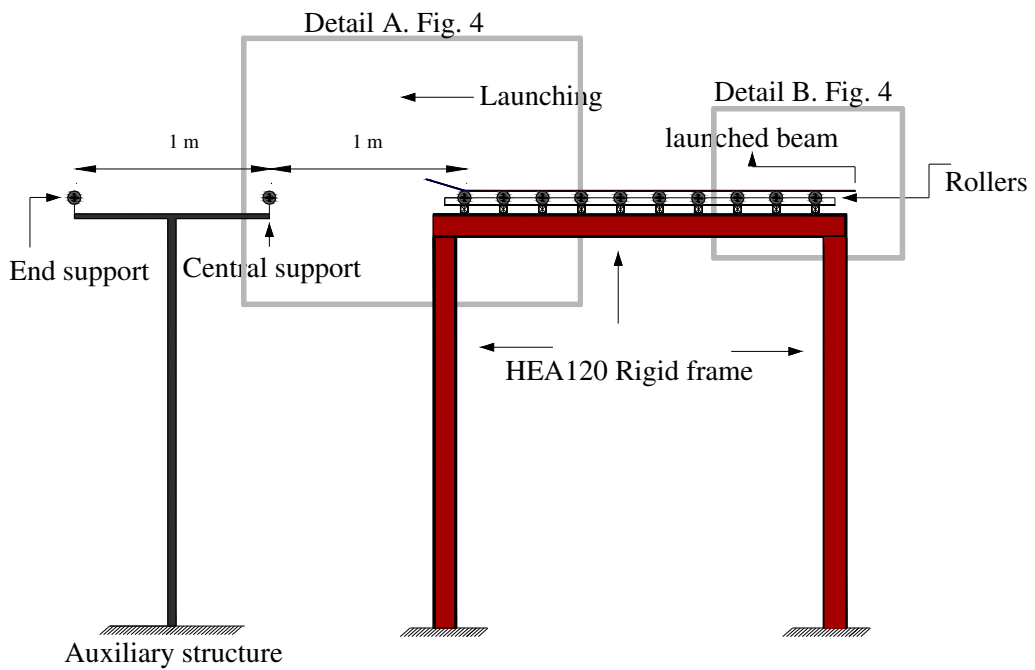
159 In its final stage, the steel plate was a symmetric two-spanned continuous beam with a total
160 length of 2000 mm and a rectangular 60mm·4mm cross section. This section is chosen for the
161 sake of accomplishing the scale of the inertia (an I-beam would provide a major-axis inertia that
162 would require a longer span). The steel plate was designed with a launching nose with the same
163 cross-section and material. This plate was launched from one support another by means of a
164 roller system designed at the laboratory facilities. The length scale (pointed out in Table 2) was
165 not precisely obtained since the cross-section had to be adapted the available commercial steel
166 profiles.

167 Fig. 3 depicts the rolling system, the rigid supports that provided the central pier, the dimensions
168 of the launching nose as well as the end support. Fig. 4 shows details A and B (displayed in Fig.
169 3) of the scale-reduced launching procedure. It is worth pointing out the following features:

170

- 171 • The rolling system was frictionless.
- 172 • Lateral restraints were added to the system for the sake of avoiding lateral displacements.
- 173 • The launching nose allowed the plate to reposition once the central and/or the end
174 supports were approached by the launched steel plate.

- 175 • The launching was carried out as a series of increments with halts every 100 mm in order
176 to minimize the potential effect of vibrations (especially in advanced cantilever phases
177 prior to contact with the roller bearings).
- 178 • The test was repeated a statistically significant number of times ($n=30$) and the results
179 showed statistical consistency.

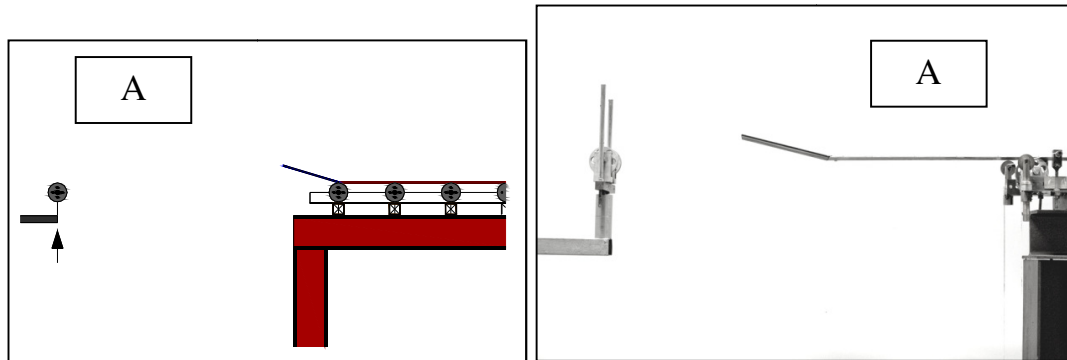


180 •

181

• **Figure 3. Laboratory test set up.**

182



183

184

• Figure 4. Details A and B of the scale-reduced model

185

186 3.2 Measurements

187 Two types of measurements were collected during the launching procedure: strains and
188 displacements at key points of the systems previously anticipated from theoretical calculations.

189 For the former, two strain gauges were bonded (longitudinally and transversely) at the point
190 where the maximum longitudinal stress was expected (precisely at the center of the steel plate,
191 see Fig. 4). The uni-axial gauges (HBM K-RY81-6) were bonded only on the upper fiber of the
192 steel plate to avoid any contact between roller and strain gauge. For the latter, the vertical
193 displacements of key points of the steel plate were collected by means of a photogrammetric
194 procedure using a HD camera. The pictures were digitalized and scaled precisely. Accurate
195 measurements were performed on the digital files. These results were further used to validate a

196 numerical model. The strain results were collected with a Spider 8 data acquisition system. The
197 signal was processed using the software CATMAN EASY 6.10 [28].

198

199

200 3.3 Experimental results

201 3.3.1 Strain

202 Fig. 5 shows the results concerning the strain evolution on the top fiber of the steel plate during
203 incremental procedure. The procedure as well as the plot are divided into five stages for
204 readability:

- 205 • Zone A: The steel plate is supported by the rollers system, the measurement equipment
206 was initialized, and the launching system was set up.
- 207 • Zone B: The launching procedure starts and the plate behaves like a cantilever with the
208 upper fiber subjected to tensile stresses (positive in the plot). The maximum level of
209 strain collected at this stage was $264\mu\text{m/m}$ before the launching nose reached the central
210 supports. Assuming that the Hooke's law governs the relationship between stresses and
211 strain of the steel plate, the maximum stress recorded at this stage was approximately 54
212 N/mm^2 .
- 213 • Zone C: The launching nose approaches the central support. The structural scheme
214 suddenly changes and sign reversals of the internal forces are observed. During this stage
215 the plate undergoes a sign reversal that ranges from the maximum tensile strain to the
216 maximum compression strain at the top fiber (negative in the plot).

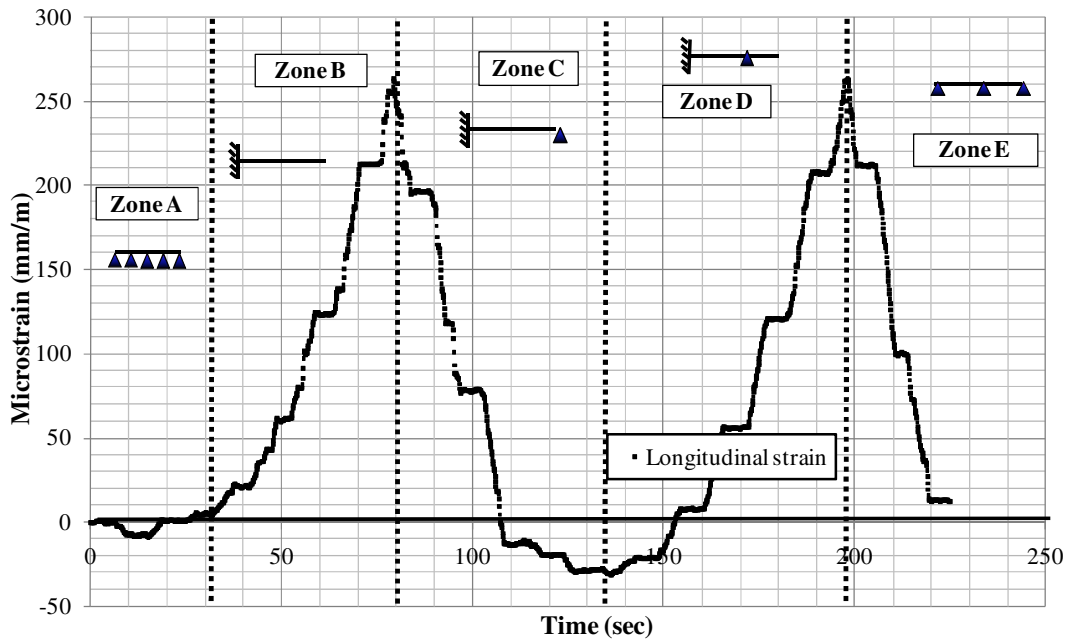
217 • Zone D: The launching procedure is continuously updated by the transient support
218 conditions and the length of the cantilever which is formed at the second span. The
219 longitudinal strain reaches a value of $264\mu\text{m/m}$ (approximately 58 Mpa of tensile on the
220 top fiber) as it approaches the end support.

221 • Zone E: The launching nose reaches its final configuration. The steel plate forms a
222 continuous two-spanned beam. It is worth mentioning that at this stage the registered
223 strain level is considerably lower than the strain level recorded during launching. This
224 fact shows the importance of a prior detailed structural analysis that depicts the launching
225 procedure.

226

227 It is worth pointing out that as the stepwise nature of the experimentally collected data comes as
228 a result of the elapsed time between successive increments of the experimental incremental
229 launching procedure.

230



231

232

Figure 5. Strain evolution at the upper fiber of the steel plate during the launching.

233

234 3.3.2 Vertical displacements

235 Fig. 6 shows the schematic procedure that has been used for tracking the vertical displacement of

236 the monitored point. The procedure consisted of placing a fixed HD camera that was shot

237 regularly by means of a time-lapse application. The series of pictures were exported and treated

238 with a CAD tool that allowed to measure the location of the monitored point with a high level of

239 accuracy. Fig. 7 shows the tracked vertical displacement at every step of 100 mm. In addition,

240 the theoretical results of the vertical displacement of a similar system (the inclination of the

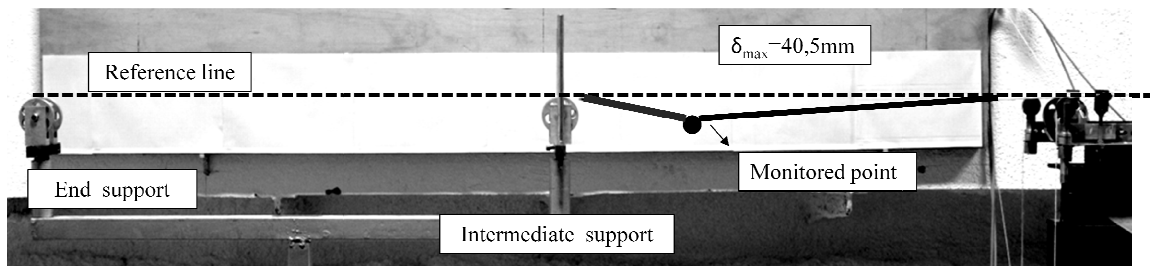
241 launching nose of such system was disregarded for simplicity) are included within the plot.

242 These theoretical results are based upon a classical Bernoulli beam formulation.

243 In Fig. 7, it is observable that the maximum deflection was registered during the zone B, at

244 which the plate acts as a cantilever. The maximum measured vertical displacement is 40,5 mm.

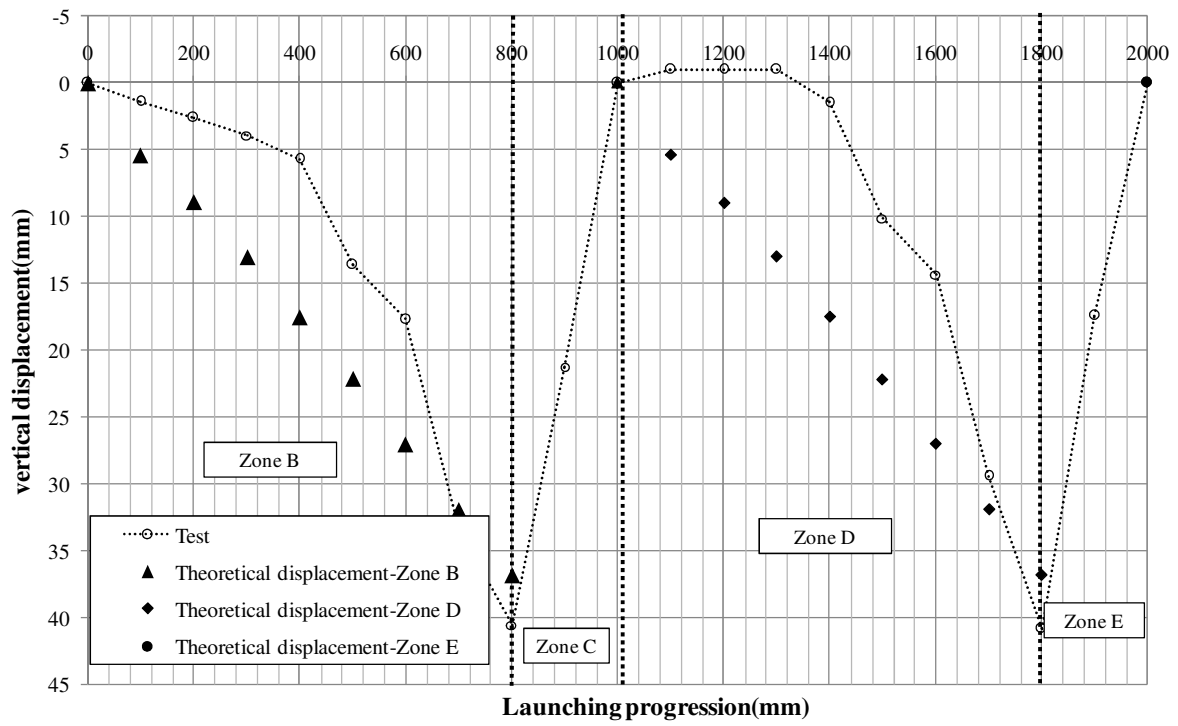
245 At this point, the theoretical value calculated for a cantilever beam using the elasticity theory is
246 38mm. The difference is attributable to the boundary conditions idealized in theory (fully
247 restrained length of the beam while placed on the roller system) as well as to the simplification
248 of the flat launching nose. The experimental test showed that at maximum cantilever stages, the
249 steel plate is not fully supported by the rollers since some gaps were observed (Fig. 8).
250 Consequently, the experimentally measured deflection was greater than the one anticipated by
251 the theoretical analysis. Further details concerning the description of the experimental results are
252 given in [29].



253

254

Figure 6. Vertical displacement at monitored point.

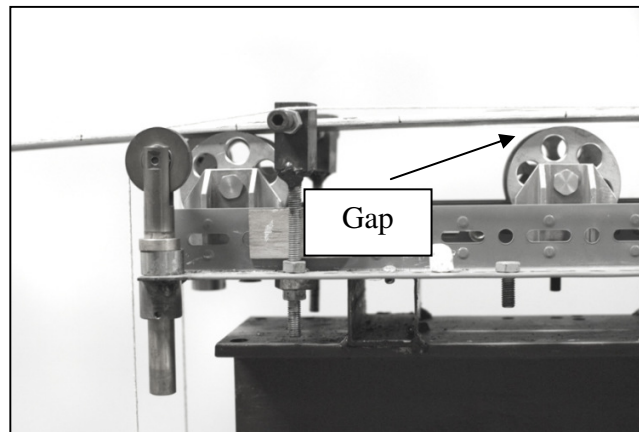


255

256

257

Figure 7. Elastic curve at monitored point.



258

259

260

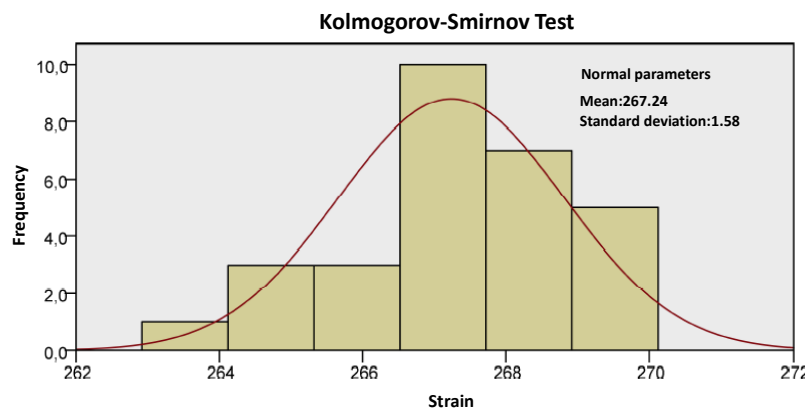
261

Figure 8. Observable gaps on top of the rollers

262 3.3.3 Statistical consistency

263 A total number of 30 tests were performed. Using the non-parametric Kolmogorov-Smirnov test
264 [30] (K-S) for the maximum strain values obtained at the tracked point in Fig. 6, the sample
265 fitted adequately with a normal distribution. Therefore the following statistics: mean, standard
266 deviation and variation coefficient were used to describe the experimental sample (Fig. 9). It is
267 observable that the obtained values of maximum strain were reasonably centered on $267\mu\text{m/m}$

268



269

270 **Figure 9. Frequency of the obtained values (maximum recorded microstrain).**

271 **4. Numerical reproduction of the scaled-reduced ILM**

272 4.1 Numerical model

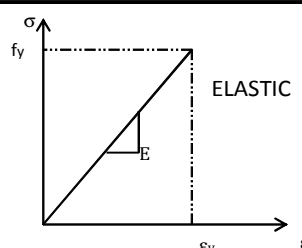
273 A numerical model implemented in the multi-purpose commercial Software Abaqus-Simulia
274 [31] was used as a numerical simulation tool. The numerical model is based upon FEM and is
275 able to reproduce a vast spectrum of physical phenomena. In this particular case, the numerical
276 model was expected to reproduce a multi-body physical problem that involved a mechanical
277 interaction between the steel plate and the support conditions (the rollers). Two features

278 characterize the modeling of the phenomenon: The geometrical nonlinearity of the problem and
279 the contact-based formulation of the system.

280 Several approaches for modeling such mechanical problem were performed throughout the
281 development of the research work [29]. Namely, the approaches included 3D bricks, shells and
282 also beam elements. These approaches differed in various degrees of computational cost,
283 accuracy, collected data and ease of modeling. Finally, the chosen numerical model was the
284 simplest and less expensive computationally. The chosen model provided a reasonably high level
285 of accuracy when balanced with the amount of collected data, the computational cost, and the
286 usefulness of the results obtained for control and monitoring purposes of incrementally launched
287 steel bridges. Other models (including shells) are under further development and may eventually
288 be useful for monitoring instability-related problems during launching.

289 The steel plate was modeled with first-order beam elements. The rollers and supports were
290 modeled as analytical, rigid and frictionless surfaces on which the steel plate was able to slide
291 and/or transmit contact stresses but conversely, was not able to penetrate through. These
292 analytical surfaces were geometrically defined as semicircular objects rigidly connected to the
293 ground. Mathematically, this contact problem is commonly referred to as the penalty-based
294 method. Further mathematical background behind this procedure is available in [29] and in the
295 Software manuals [31]. A convergence analysis by comparing theoretical and experimental
296 values to the numerically obtained ones was also performed. The beam model proved relatively
297 low mesh-dependent. Table 3 shows the principal characteristics of the model, which is simple
298 and straightforward.

299

Numerical simulation	
Software	Abaqus
Solver	Abaqus-Standard
Cross-section	60 mm x 4 mm
Material	Steel
E (N/mm ²)	210000
Density (Kg/m ³)	7850
Constitutive equation (Elastic)	
Procedure	Geometrically nonlinear
Contact-Friction	Penalty-based contact.
Interaction	Tangentially: Frictionless Normally: No penetration but separation
Load type	Self-weight
Beam element	B21 first-order, planar
$L_{\text{span, scale-reduced}}$ (mm)	2000
Mesh	Uniform. Length= $L_{\text{beam}}/200$
Bearings	Semi-circular rigid wires

301

302

Table 3. Characteristics of the numerical model (see Abaqus manuals [29][31])

303

304 Fig. 10 displays a lateral view of the numerical reproduction of the scale-reduced test. The point

305 1 is located precisely at the same position than the strain gauges bonded in the steel plate.

306 Consequently, the strain measurements could be compared. The point 2 is located at the

307 beginning of the launching nose and the displacement results (vertical) were compared to those

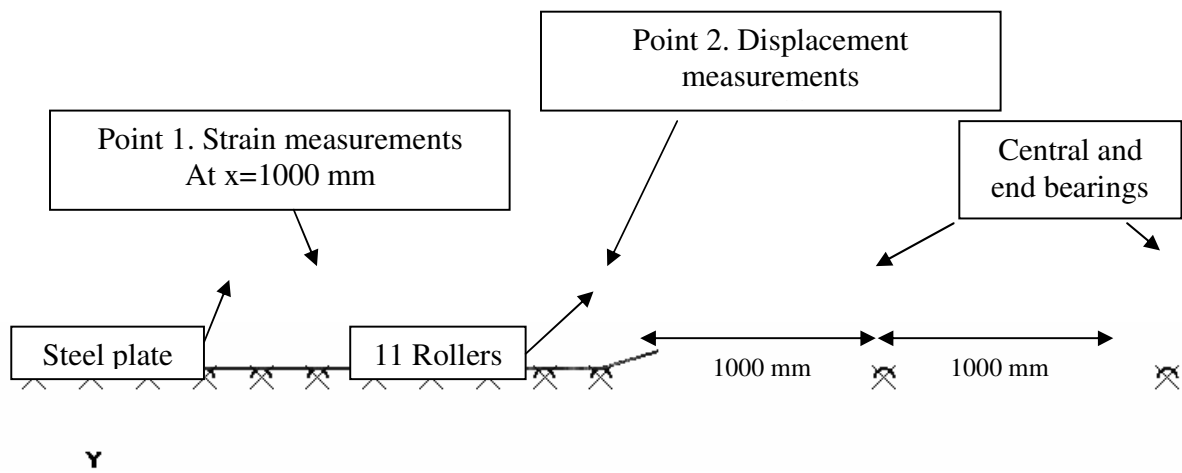
308 measured at the lab. The numerical model includes thus, a steel plate, 11 rollers as well as the
309 central and end bearings (of the same numerical nature than the rollers).

310

311

312

313



314

315

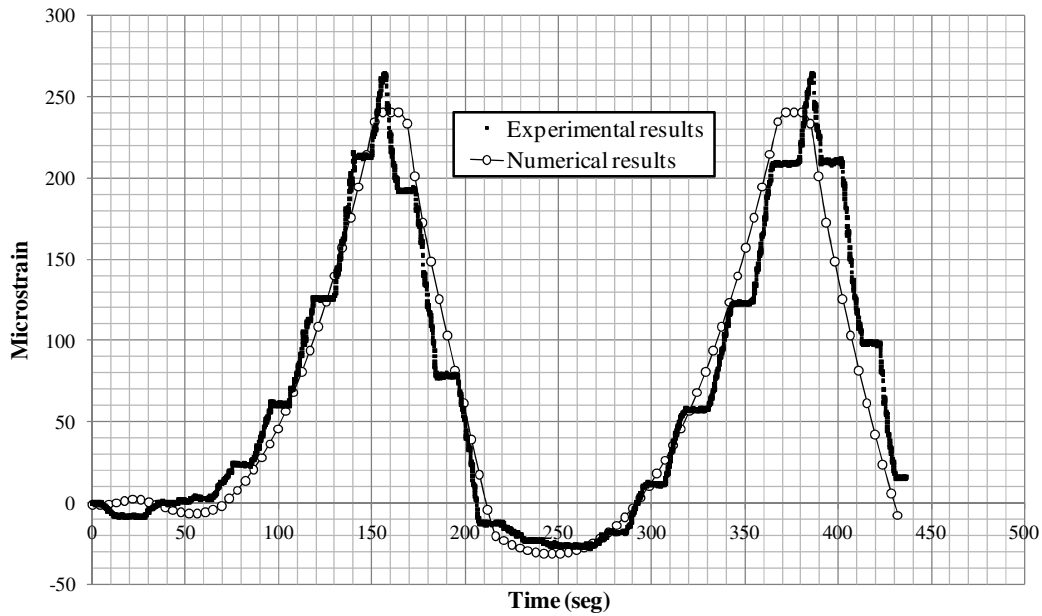
Figure 10. Numerical reproduction of the scale-reduced test. Lateral view.

316

317 4.2 Validation of the numerical model

318 The numerical model was validated by reproducing precisely the experimental test depicted in
319 section 3. The experimentally collected data related to strain and vertical displacements was used
320 as a benchmark. The numerical model including the characteristics depicted in Table 3 provided
321 similar results related to strain and vertical displacement as the steel plate was numerically
322 launched. Fig. 11 displays the comparison between the experimental and the numerical results
323 related to the longitudinal strain of the steel plate at the depicted point 1. Both curves practically
324 coincide (stepwise nature of the experimental results aside). The numerical model reproduces
325 quite satisfactorily the response observed experimentally both qualitatively and quantitatively. A

326 slight difference between the maximum strain values at both monitored peaks is observable. This
327 difference is attributed to the greater flexibility of the experimental test (Fig. 8)



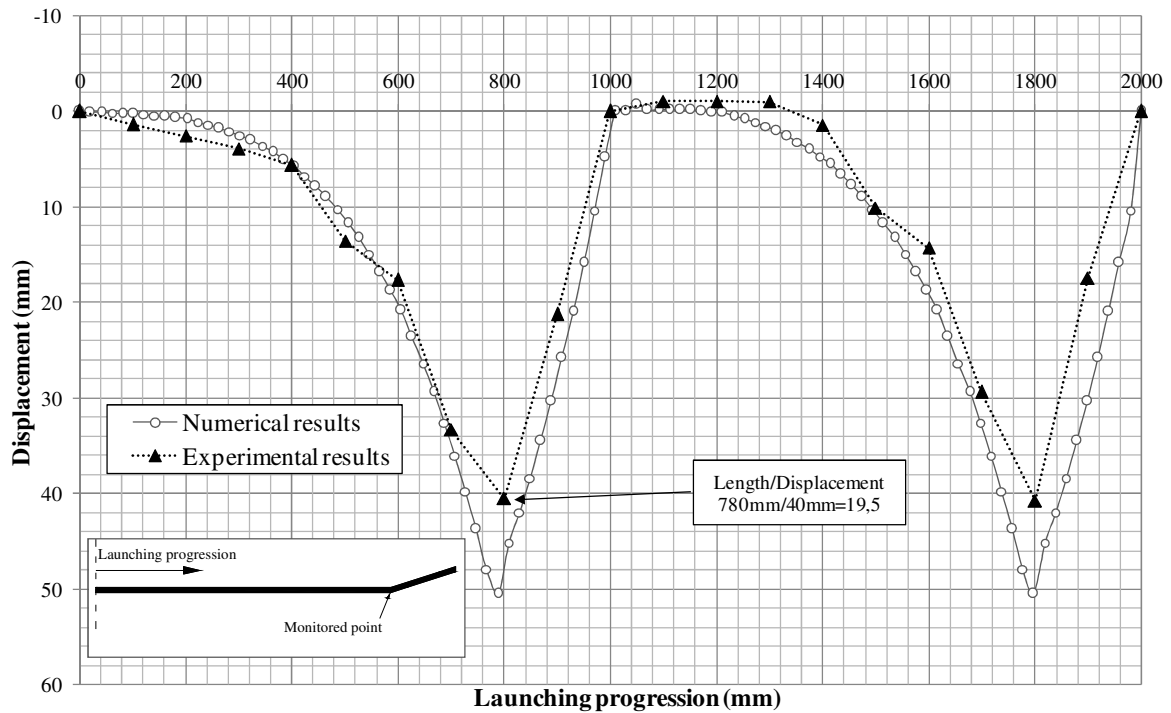
328

329

Figure 11. Numerical vs. experimental results related to longitudinal strain

330 Fig. 12 displays a comparison between the experimental and the numerical results related to the
331 vertical displacement of the steel plate at the depicted point 2. Both curves practically coincide
332 qualitatively but there is a difference in quantitative terms when compared to the strain results at
333 peak points. The differences are, however, rather small. The numerical model yields a slightly
334 more flexible response than the experimental data.

335 The main novel feature of the numerical model, which is the contact-based formulation between
336 the rollers and the girders, is adequately reproduced.



337

338

Figure 12. Numerical VS experimental-Vertical displacement.

339

340

341 5. Numerical reproduction of a real scale incrementally launched bridge

342 A numerical reproduction of a hypothetical ILM of the steel bridge depicted in Fig. 2 was

343 performed with the validated model. The numerical characteristics of such model are identical to

344 those depicted in Table 3. There is, though, a difference worth mentioning: the bearings in this

345 model were created according to the standard dimensions for these devices [23]. These elements

346 were equally modeled as analytical, rigid surfaces. In this case, a regular mesh of 186 first-order

347 beam elements (B21, whose length equals approximately the relationship $L_{span}/200$) was

348 deployed. The configuration of the launched structure is identical to the one depicted in Fig. 10
349 but in this case, $L=75000$ mm.

350 The numerical model allows the user to extract any kind of information related to the stress,
351 strain, displacement and the contact forces fields. This represents a vast amount of data, which is
352 not necessarily useful during the construction stages. In field bridge engineering, it might be of
353 great usefulness to accurately anticipate the forces, strains and displacements the girder
354 undergoes during the incremental launching procedure. Consequently, the results that are
355 displayed herein are aimed at showing the potential control tools such simulation may provide.
356 Therefore, three structural results are monitored and depicted:

- 357 • Strains at point A (exact middle point of the girder).
- 358 • Vertical displacement at the front of the cantilever
- 359 • Reaction forces at central and end bearings.

360 The abovementioned magnitudes are usually monitored during the launching phase. A thorough
361 comparison between the anticipated values and the field measurements may clarify and/or
362 confirm the correct practice of the launching process or potentially, may prevent undesired
363 problems during construction.

364

365

366 5.1 Strains

367 The results concerning stresses and strains are useful in a twofold fashion:

368 • For design purposes, the model may warn about any potential yielding of the girder
369 during the ILM if the strain is associated with the constitutive equation of the material.

370

371 • For control purposes, the results related to strains may be compared with in situ
372 measurements that are increasingly used nowadays [20-23].

373 For the former, localized yielding of the steel girders during launching is highly undesired. The
374 numerical model provides information that may anticipate any potential yielding of the girder at
375 any point. The numerical model may flag any finite element that overpasses a defined threshold
376 of stresses (namely, the yield stress f_y). The yielded areas could be pinpointed at the end of the
377 procedure and the design of the steel girder may be changed at design stages.

378 For the latter, the model allows to track the strain at any given point of interest (that may be the
379 points at which strain gauges are located). The stress levels may also be inferred from the strain
380 field via the constitutive equation (which is reasonably expected to be linear during
381 construction).

382 Fig. 13 displays a control plot of strain and stresses obtained with the numerical simulation of the
383 ILM. The strain-stress values are obtained from point A, which is located where the maximum
384 longitudinal stress occurs.

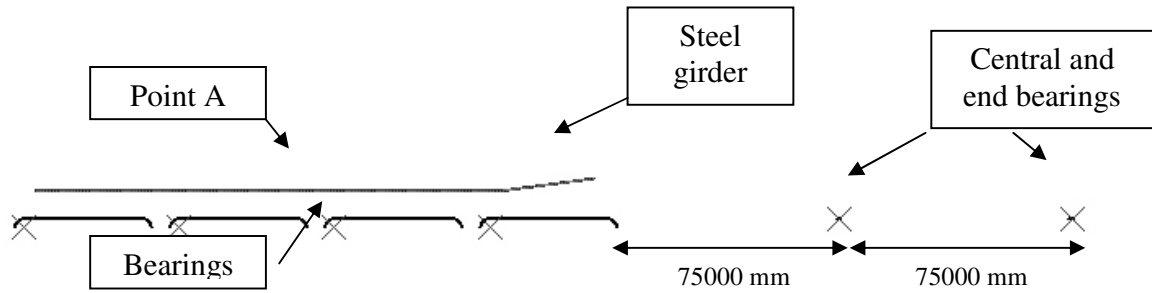
385 Noticeably, sign reversals are observable since the girder undergoes consecutive sagging and
386 hogging bending moments. This information should reasonably coincide with the field
387 measurements. Finally, the plot includes thresholds that define warning areas of undesired levels
388 of stress and strain (pinpointed qualitatively in the plot).

389

390

391

392



393

394

Fig 13. Numerical reproduction of the ILM

395

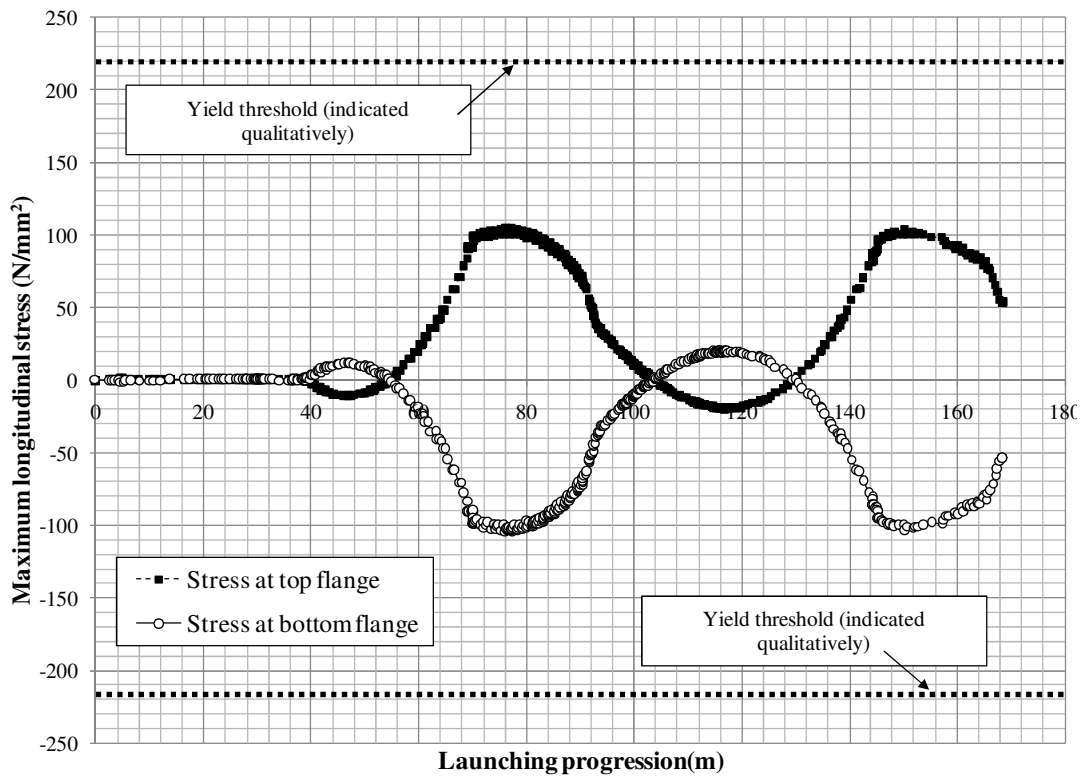
396 5.2 Vertical displacements

397 The vertical displacements of the steel girders are generally monitored and controlled in situ with
398 basic topographic equipment. These measurements do not require complex acquisition data
399 systems despite the high level of accuracy provided by modern total stations. The contractors,
400 designers and bridge owners often rely on such measurements due to their adequate balance
401 between accuracy and ease. Any individual involved in the construction can track the
402 progression of the launching in terms of deflection of the steel girder.

403 Fig. 14 displays the history of the vertical displacement of the point referred to as B in the plot
404 obtained with the numerical model. This history should be read as follows, for a given distance x
405 (mm) of the tracked point during launching, its vertical displacement is given. Noticeably, the
406 displacement increases in sagging zones and decreases as the girder passes over a given bearing.

407 Field measurements and numerical predictions may also be compared and thus, conclusions
408 related to the process may be drawn.

409



410

411 **Figure 14. Longitudinal stress control at point A.**

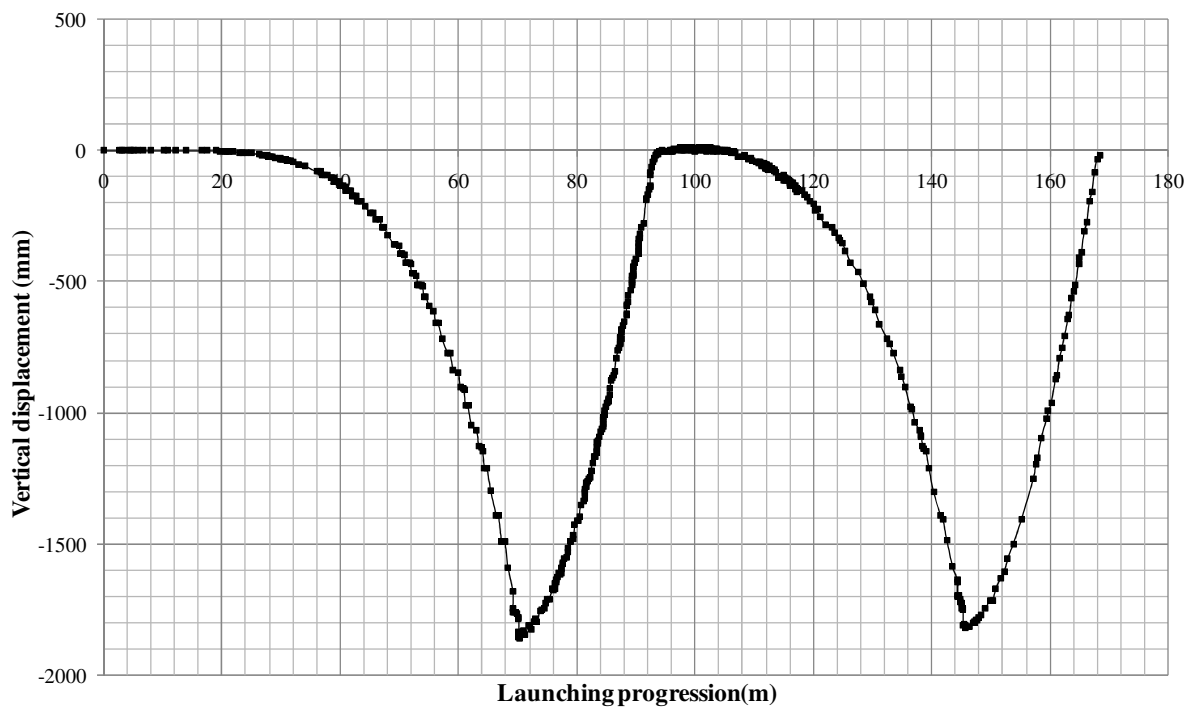
412

413 5.3 Reaction force at the bearings

414 Load cells are usually deployed at bearing during launching [32]. These measurements allow to
415 monitor the magnitude of the reaction forces. In bridges with multi-girder cross-sections, these
416 measurements are of the utmost importance for the verification of the adequate position of the
417 bridge during launching. All load cells provided at a given bearing should read a proportional
418 amount of the total load which is known beforehand. If an undesired loss of symmetry occurs

419 during launching, the reactions forces would differ considerably from one girder to another. This
420 implies repositioning of the bridge with all costs and time-waste associated. .

421 The numerical model provides information related to the contact stresses transmitted from the
422 girders to the bearing. In addition, it provides information related to the internal forces that occur
423 at the girder (bending moment, shear). Fig. 15 displays a reaction force graph plotted against the
424 distance at which the launching nose is located (namely, the launching progression). The results
425 might be compared with in situ measurements for control purposes but also, these results might
426 be used at design stages. In steel launched bridges, it is well-known that the patch loading forces
427 combined with the bending moments are, among others, important forces to be verified.



428

429 **Figure 15. Vertical displacement control of a real-scale launched steel bridge.**

430

431

Figure 15. Vertical reaction control at central pier and end abutment.

432 **6. Conclusions**

433 In this paper, experimental and numerical models aimed at simulating the structural behavior of a
434 steel I-girder bridge constructed by the incremental launching method (ILM) are depicted.

435 On the one hand, the experimental test has been performed in a scale-reduced fashion and has
436 been useful for validation purposes. On the other hand, the numerical model using beam
437 elements proves versatile when simulating the launching process within a short calculation time.
438 The numerical model includes a contact-based formulation which reproduces satisfactorily the
439 transient support conditions that occur during the ILM.

440 The numerical simulation of the ILM represents a useful tool for monitoring and controlling the
441 various magnitudes that are typically measured in situ with traditional field equipment. This
442 numerical control allows bridge designers, contractors and owners to anticipate the structural
443 response of the steel girders. Results related to the strain-stress field, vertical displacements and
444 reaction forces at bearings might be easily inferred from the simulation and compared to field
445 measurements. The proposed simulation of the ILM model provides an adequate balance
446 between accuracy, collected data and ease. The simulation presented herein might be extended to
447 box girders or other bespoke cross-sections.

448

449 **7. References**

450

451 [1] LaViolette M., Wipf T., Lee Y. Bridge construction practices using incremental launching,
452 American Association of State Highway and Transportation Officials, AASHTO, 2007.

453

454 [2] Rosignoli M. Bridge Launching, Thomas Telford, 2002.

455

456 [3] Baur W., Bridge Erection by Launching is Fast, Safe and Efficient, Civil Engineering –
457 ASCE, Vol. 47 (3), 1977.

458

459 [4] Gohler B. Pearson P., Incrementally Launched Bridges. Design and Construction,
460 Ernst and Sohn, Berlin, Germany, 2000.

461

462 [5] Alistair P., Large and Small Incrementally Launched Structures, Transportation Research
463 Record 1696 (5B0060), Transportation Research Board, Washington D.C., 2000.

464

465 [6] Zellner, W. and Svensson, H. . Incremental Launching of Structures. Journal of Structural
466 Engineering. Vol 109 (2), 520–537. 1983

467

468

469 [7] Rosignoli M., Site Restrictions Challenge Bridge Design, Concrete International, Vol. 20 (8),
470 1998.

471

472 [8] Rosignoli M. Pre-sizing of Prestressed Concrete Launched Bridges. ACI Structural Journal.
473 Vol. 96 (5), pp. 705-711, 1999.

474

475 [9] Rosignoli M. Nose-Deck Interaction in Launched Prestressed Concrete Bridges. Journal of

476 Bridge Engineering, Vol 3 (1) pp. 21-27. 1998.

477

478 [10] Rosignoli M. Reduced-Transfer-Matrix Method of Analysis of Launched Bridges. ACI
479 Structural Journal, Vol. 96 (4). pp. 603-608. 1999.

480

481 [11] Rosignoli M., Monolithic Launch of the Reggiolo Overpass, Concrete International, Vol. 29
482 (2), 2001.

483

484 [12] Granath P., Distribution of support reaction against a steel girder on a launching shoe,
485 Journal of Constructional Steel Research, Vol 47 (3), pp. 245-270. 1998

486

487 [13] Granath P., Thorsson A., Edlund B., I-shaped steel girders subjected to bending moment and
488 travelling patch loading, Journal of Constructional Steel Research, Vol 54 (3), pp. 409-421. 2000

489

490 [14] Granath P., Serviceability limit state of I-shaped steel girders subjected to patch loading,
491 Journal of Constructional Steel Research, Vol. 54 (3), pp. 387-408. 2000

492

493 [15] Favre R., Badoux M., Burdet O., Laurencet P., Incremental Launching for the Ile Falcon
494 Bridge, Concrete International, Vol. 21 (2), February 1999.

495

496 [16] Hewson N., Hodgkinson A., Incremental Launch of Brides Glen Bridge, Ireland,
497 Concrete, Vol. 38 (7), 2004

498

499 [17] Zhuravov L., Chemerinsky O., Seliverstov V., Launching Steel Bridges in Russia, Journal
500 of International Association for Bridge and Structural Engineering (IABSE), Vol. 6 (3), pp. 183-
501 186. 1996

502

503 [18] Marzouk M., El-Dein H., El-Said M., Application of computer simulation to construction of
504 incrementally launching bridges, Journal of Civil Engineering and Management, Vol. 13 (1), pp:
505 27-36. 2007

506

507 [19] Rongqiao X, Binlei Shao. A new beam element for incremental launching of bridges,
508 Journal of Bridge Engineering, pp: 1-19. 2011

509

510 [20] Chacón R., Guzmán F., Mirambell E., Real E., Oñate E. Wireless Sensor Networks for
511 strain monitoring during steel bridges launching, International Journal of Structural Health
512 Monitoring, Vol 8 (3), pp: 195-205, 2009

513

514

515 [21] Wipf T., Phares B., Abendroth R., Chang B., Abraham S., Monitoring of the
516 Launched Girder Bridge over the Iowa River on US 20, Final Report CTRE Project 01-108,
517 Center for Transportation Research and Education, Iowa State University. March 2004.

518

519 [22] Lebet J. Measurements taken during the launch of the 130 m Span Vaux Viaduct,
520 Steelbridge, OTUA. Millau, France. (2004)

521 [23] Zhang Y., Luo R. Patch loading and improved measures of incremental launching of steel
522 box girder. Journal of Constructional Steel Research. Vol 68 (1), pp:11-19. 2012
523

524 [24] Martins O.P., Sampaio A.Z., Bridge launching construction visualized in a virtual
525 environment. The International Journal of Virtual Reality. Vol. 10 (2), pp: 49-56. 2011.
526

527 [25] Combri Design Manual –Part I Applications of Euro Code rules, first edition, 2008.
528

529 [26] Buckingham E., On physically similar systems. Illustrations of the use of dimensional
530 equations. Physical Review, Vol. 4, pp: 345-376. 1914.
531

532 [27] Blanco E., Oller S., Gill L. Análisis Experimental de estructuras, CIMNE, Barcelona, Spain,
533 2007 (in spanish)
534

535 [28] CATMAN Easy V 6.10. Hottinger Baldwin Messtechnik HBM 2012.
536

537 [29] Uribe N., Reproducción numérica y experimental del proceso de lanzamiento de un puente
538 metálico por empujes sucesivos. Master's Thesis. Construction Engineering Department.
539 ETSICCPB. Universitat Politècnica de Catalunya. 2012 (in spanish)
540 <http://upcommons.upc.edu/pfc/handle/2099.1/14898>
541

542 [30] Lindgren B.W., Statistical theory 2nd Edition, The Mcmillan Company, New York, 1962.
543

544 [31] Abaqus FEA, Simulia© V6.10.3. Dassault Systèmes. 2012.

545

546 [32] Marzouk M., Said H., El-Said M., Framework for multiobjective optimization of launching
547 girder bridges. Journal of Construction Engineering and Management. Vol 135 (8), pp 791-800.

548 2011